Atmos. Chem. Phys., 17, 1297–1311, 2017
www.atmos-chem-phys.net/17/1297/2017/
doi:10.5194/acp-17-1297-2017

Atmospheric Chemistry and Physics
Open Access
EGU

Influence of enhanced Asian NO_x emissions on ozone in the upper troposphere and lower stratosphere in chemistry–climate model simulations

Chaitri Roy[1], Suvarna Fadnavis[1], Rolf Müller[2], D. C. Ayantika[1], Felix Ploeger[2], and Alexandru Rap[3]

[1]Indian Institute of Tropical Meteorology, Pune, India
[2]Forschungszentrum Jülich GmbH, IEK7, Jülich, Germany
[3]School of Earth and Environment, University of Leeds, Leeds, UK

Correspondence to: Suvarna Fadnavis (suvarna@tropmet.res.in)

Received: 5 July 2016 – Published in Atmos. Chem. Phys. Discuss.: 20 July 2016
Revised: 29 December 2016 – Accepted: 9 January 2017 – Published: 27 January 2017

Abstract. The Asian summer monsoon (ASM) anticyclone is the most pronounced circulation pattern in the upper troposphere and lower stratosphere (UTLS) during northern hemispheric summer. ASM convection plays an important role in efficient vertical transport from the surface to the upper-level anticyclone. In this paper we investigate the potential impact of enhanced anthropogenic nitrogen oxide (NO_x) emissions on the distribution of ozone in the UTLS using the fully coupled aerosol–chemistry–climate model, ECHAM5-HAMMOZ. Ozone in the UTLS is influenced both by the convective uplift of ozone precursors and by the uplift of enhanced-NO_x-induced tropospheric ozone anomalies. We performed anthropogenic NO_x emission sensitivity experiments over India and China. In these simulations, covering the years 2000–2010, anthropogenic NO_x emissions have been increased by 38 % over India and by 73 % over China with respect to the emission base year 2000. These emission increases are comparable to the observed linear trends of 3.8 % per year over India and 7.3 % per year over China during the period 2000 to 2010. Enhanced NO_x emissions over India by 38 % and China by 73 % increase the ozone radiative forcing in the ASM anticyclone (15–40° N, 60–120° E) by 16.3 and 78.5 mW m^{-2} respectively. These elevated NO_x emissions produce significant warming over the Tibetan Plateau and increase precipitation over India due to a strengthening of the monsoon Hadley circulation. However, increase in NO_x emissions over India by 73 % (similar to the observed increase over China) results in large ozone production over the Indo-Gangetic Plain and Tibetan Plateau. The higher ozone concentrations, in turn, induce a reversed monsoon Hadley circulation and negative precipitation anomalies over India. The associated subsidence suppresses vertical transport of NO_x and ozone into the ASM anticyclone.

1 Introduction

Rapid economic development and urbanization in Asia has resulted in an unprecedented growth in anthropogenic emissions of nitrogen oxides (NO_x), carbon monoxide (CO), carbon dioxide (CO_2), and methane (CH_4). Many of these species affect concentrations of tropospheric ozone, which is both an important polluting agent and a greenhouse gas (Wild and Akimoto, 2001; Chatani et al., 2014; Revell et al., 2015). Ground-based and satellite observations show a large amount of these ozone precursors concentrated over India and China (Sinha et al., 2014; Richter et al., 2005; Jacob et al., 1999; Zhao et al., 2013; Gu et al., 2014). Studies show that tropospheric ozone production over Asia is controlled by the abundance of NO_x and volatile organic carbon (VOC) (Sillman, 1995; Lei et al., 2004; Zhang et al., 2004; Tie et al., 2007), with large regions such as India and China being NO_x limited regions. Therefore, increased NO_x in these regions leads to an increase in ozone concentrations (Yamaji et al., 2006; Sinha et al., 2014; Fadnavis et al., 2015). Recently, positive trends in Asian tropospheric column NO_2 have been reported, i.e. 3.8 % yr^{-1} over India, using Scanning Imaging Absorption SpectroMeter for Atmo-

spheric Chartography (SCIAMACHY) observations for the period 2003–2011 (Ghude et al., 2013) and 7.3 % yr^{-1} over China using Ozone Monitoring Instrument (OMI) observations for the period 2002–2011 (Schneider and van der A, 2012). Lightning contributes to the production of NO_x in the middle and upper troposphere (Barret et al., 2016). Over the Asian region, lightning contributes ~ 40 % to NO_x and 20 % to ozone production in the middle and upper troposphere during the monsoon season (Tie et al., 2001; Fadnavis et al., 2014). The upper-tropospheric ozone concentration is determined by in situ production from both lightning and ozone precursors, which are transported from the boundary layer (Søvde et al., 2011; Barret et al., 2016).

Tropospheric ozone has a warming effect on climate, its estimated radiative forcing due to increased concentrations since pre-industrial times being 0.4 W m^{-2}, with a 5 to 95 % confidence range of 0.2 to 0.6 W m^{-2} (Stevenson et al., 2013; Myhre et al., 2013). Previous studies highlighted the importance of the tropical tropopause region for ozone radiative forcing (Lacis et al., 1990; Riese et al., 2012; Rap et al., 2015) and showed that ozone perturbations exert a large influence on the thermal structure of the atmosphere (e.g. Thuburn and Craig, 2002; Foster et al., 1997). A recent study based on Atmospheric Chemistry and Climate Model Intercomparison Project (ACCMIP) models reported that NO_x and CH_4 are the greatest contributors in determining tropospheric ozone radiative forcing (Stevenson et al., 2013).

Asian summer monsoon (ASM) convection efficiently transports Asian pollutants from the boundary layer into the upper troposphere and lower stratosphere (UTLS) (Randel and Park, 2006; Randel et al., 2010; Fadnavis et al., 2013, 2014). Studies pertaining to modelling and trajectory analysis confirm this finding (Li et al., 2005; Park et al., 2007; Randel et al., 2010; Chen et al., 2012; Vogel et al., 2015, 2016). Satellite observations show the confinement of a number of chemical constituents like water vapour (H_2O), CO, CH_4, ethane, hydrogen cyanide (HCN), peroxyacetyl nitrate (PAN), and aerosols within the ASM anticyclone (Park et al., 2004, 2007, 2008; Li et al., 2005; Randel and Park, 2006; Xiong et al., 2009; Randel et al., 2010; Lawrence, 2011; Abad et al., 2011; Fadnavis et al., 2013, 2014, 2015; Barret et al., 2016), which has potential implications on stratospheric chemistry and dynamics. Thus the rise in anthropogenic emissions over the ASM region alters the chemical composition of the UTLS (Lawrence, 2011; Fadnavis et al., 2014, 2015) during the monsoon season. Another prominent feature of the satellite observations is an ozone minimum in the ASM anticyclone (near 100 hPa) (Gettelman et al., 2004; Konopka et al., 2010; Braesicke et al., 2011). This ozone minimum is linked to upward transport of ozone-poor air masses (Gettelman et al., 2004; Park et al., 2007; Kunze et al., 2010). Observations show that convectively lifted air masses arriving in the anticyclone are ozone poor but rich in ozone precursors. Balloon sonde observations show that ozone variations near the anticyclone are strongly correlated with temperature near the tropopause (Tobo et al., 2008). Thus the linkage of low ozone and high concentrations of ozone precursors with the temperature variation in the anticyclone is an open question.

In this study we ask the question of how increasing Asian NO_x emissions and the associated ozone production affect ozone radiative forcing and monsoon circulation. We perform sensitivity experiments of increased anthropogenic NO_x emissions using the state-of-the-art ECHAM5-HAMMOZ (European Centre General Circulation Model version 5) chemistry–climate model (Roeckner et al., 2003; Horowitz et al., 2003; Stier et al., 2005). We estimate the ozone radiative forcing for the different anthropogenic NO_x emission scenarios, together with associated changes in temperature and the monsoon circulation. The paper is organized as follows: in Sect. 2 the data and model set-up are described, the results are summarized in Sect. 3 and discussed in Sect. 4, and the conclusions are given in Sect. 5.

2 Data description and model set-up

2.1 Satellite measurements

Earth Observing System (EOS) microwave limb sounder (MLS) is one of the four instruments on NASA's EOS Aura satellite flying in the polar sun-synchronous orbit. It measures the thermal emissions at millimetre and sub-millimetre wavelengths (Waters et al., 2006). It performs 240 limb scans per orbit with a footprint of ~ 6 km across-track and ~ 200 km along-track, providing ~ 3500 profiles per day. MLS also measures vertical profiles of temperature, ozone, CO, H_2O, and many other constituents in the mesosphere, stratosphere, and upper troposphere (Waters et al., 2006). In the UTLS, MLS has a vertical resolution of about 3 km. MLS vertical profiles of ozone show good agreements with the Stratospheric Aerosol and Gas Experiment II (SAGE-II), Halogen Occultation Experiment (HALOE), Atmospheric Chemistry Experiment (ACE), and ozonesonde measurements (Froidevaux et al., 2006). The MLS ozone profiles are considered to be useful in the range of 215–0.46 hPa (Livesey et al., 2005). In this study we analyse the MLS level 2 (version 4) ozone mixing ratios data for the period 2004–2013. The data have been gridded horizontally, within latitude bins of equal area (with the equatorial bin of 150 km width) and longitude bins of about 8.5°. These data can be accessed from http://mls.jpl.nasa.gov/. For comparison, simulated ozone is convolved with the MLS averaging kernel (Livesey et al., 2011).

2.2 Model simulation and experimental set-up

We employ the aerosol–chemistry–climate model ECHAM5-HAMMOZ, which comprises the general circulation model ECHAM5 (Roeckner et al., 2003), the

tropospheric chemistry module MOZART2 (Horowitz et al., 2003), and the aerosol module Hamburg aerosol model (HAM) (Stier et al., 2005). It includes NO_x, VOC, and aerosol chemistry. The gas-phase chemistry is based on the chemical scheme provided by the MOZART-2 model (Horowitz et al., 2003), which includes detailed chemistry of the O_x–NO_x hydrocarbon system with 63 tracers and 168 reactions. The $O(^1D)$ quenching reaction rates used are taken from Sander et al. (2006) and isoprene nitrates chemistry taken from Fiore et al. (2005). The dry deposition in ECHAM5-HAMMOZ follows the scheme given by Ganzeveld and Lelieveld (1995). Soluble trace gases like HNO_3 and SO_2 are also subject to wet deposition. In-cloud and below-cloud scavenging follows the scheme given by Stier et al. (2005). Interactive calculation of cloud droplet number concentration is according to Lohmann et al. (1999) and ice crystal number concentrations are according to Kärcher and Lohmann (2002). The convection scheme is based on the mass flux scheme developed by Tiedke (1989). Lightning NO_x emissions are parameterized following Grewe et al. (2001).

The model is run at a T42 spectral resolution corresponding to about $2.8° \times 2.8°$ in the horizontal dimension and 31 vertical hybrid $\sigma-p$ levels from the surface to 10 hPa. In our model simulations, emissions from anthropogenic sources and biomass burning are from the year 2000 RETRO project data set (available at http://eccad.sedoo.fr/) (Schultz et al., 2004, 2005, 2007, 2008). Emissions of SO_2, black carbon, and organic carbon are based on the AEROCOM-II emission inventory, also for the year 2000 (Dentener et al., 2006). The distribution of NO_x emission mass flux (kg m^{-2} s^{-1}) averaged for the ASM season (June–September) is shown in Fig. S1 in the Supplement. It shows high values over the Indo-Gangetic Plain and East China. Other details of model parameterizations, emissions, and evaluation are described by Fadnavis et al. (2013, 2014, 2015) and Pozzoli et al. (2008a, b, 2011). Each of our model experiments consists of continuous simulations for 11 years from 2000 to 2010. The base year for emissions is taken as 2000 and emissions were repeated every year throughout the simulation period. Meteorology varied due to varying monthly mean sea surface temperature (SST) and sea ice concentration (SIC). The AMIP2 SSTs and SIC varying for the period 2000–2010 were specified as a lower boundary condition.

In order to understand the impact of enhanced anthropogenic NO_x emissions on the distribution of ozone in the UTLS, sensitivity simulations were performed for the period 2000–2010. The experimental set-up is the same as described by Fadnavis et al. (2014). The four simulations analysed in this study are a reference experiment (CTRL) and three sensitivity experiments (referred to as experiments 2–4), where the anthropogenic NO_x emissions over India and China are scaled in accordance with the observed trends. In experiment 2, anthropogenic NO_x emissions are increased over India by 38 % (Ind38). In experiment 3, increases over China by 73 % (Chin73) are prescribed. In order to analyse the effects of similar NO_x percentage increases over India and China, NO_x emissions are increased over India by 73 % (Ind73) in experiment 4. The emission perturbations were obtained from observed NO_2 trends of 3.8 % per year over India (Ghude et al., 2013) and 7.3 % per year over China (Schneider and van der A, 2012). Hiboll et al. (2013) also reported similar increasing NO_x values over megacities in India and China. All four simulations use the same VOC and CO emissions and they all include NO_x production due to lightning (lightning-on) and soil emissions. There may be indirect impact of lightning NO_x emission. Since it is same in CTRL and sensitivity simulations its impact may be negligible.

In addition, a lightning-off simulation was performed for the same period and boundary conditions as experiments 1–4 (this simulation is the same as the one described in Fadnavis et al., 2014). The impact of lightning on NO_x production is estimated by comparing the CTRL (lightning-on) with lightning-off simulations.

The accuracy of the simulation of the monsoon circulation probably depends on model resolution and an increased vertical resolution may improve the model performance (Druyan et al., 2008; Abhik et al., 2014). However, the model resolution of T42L31 is capable of reasonably simulating the general regional spatial pattern of precipitation and low-level circulation (Rajeevan et al., 2005) (see Fig. S2, showing simulated seasonal mean precipitation and circulation at 850 hPa in the CTRL simulation).

The heating rates and radiative forcings associated with the ozone changes in our three sensitivity simulations are calculated using the Edwards and Slingo (1996) radiative transfer model and the fixed dynamical heating approximation for stratospheric temperature adjustment. Similarly to previous studies (Riese et al., 2012; Bekki et al., 2013; Rap et al., 2015), we used the offline version of the model, with six shortwave and nine longwave bands, and a delta-Eddington two-stream scattering solver at all wavelengths.

3 Results

3.1 Comparison with MLS satellite measurements in the UTLS

The spatial distributions of ozone mixing ratios from MLS observations at 100 hPa and from the CTRL ECHAM5-HAMMOZ simulation at 90 hPa (the nearest model level) after smoothing with the averaging kernel of MLS are illustrated in Fig. 1a and b respectively. For comparison we have interpolated the model data to the MLS pressure grid, then applied the MLS averaging kernel and finally interpolated back to the model pressure grid. The climatological horizontal winds plotted in the figure clearly show the anticyclonic upper-level monsoon circulation. Recent attempts

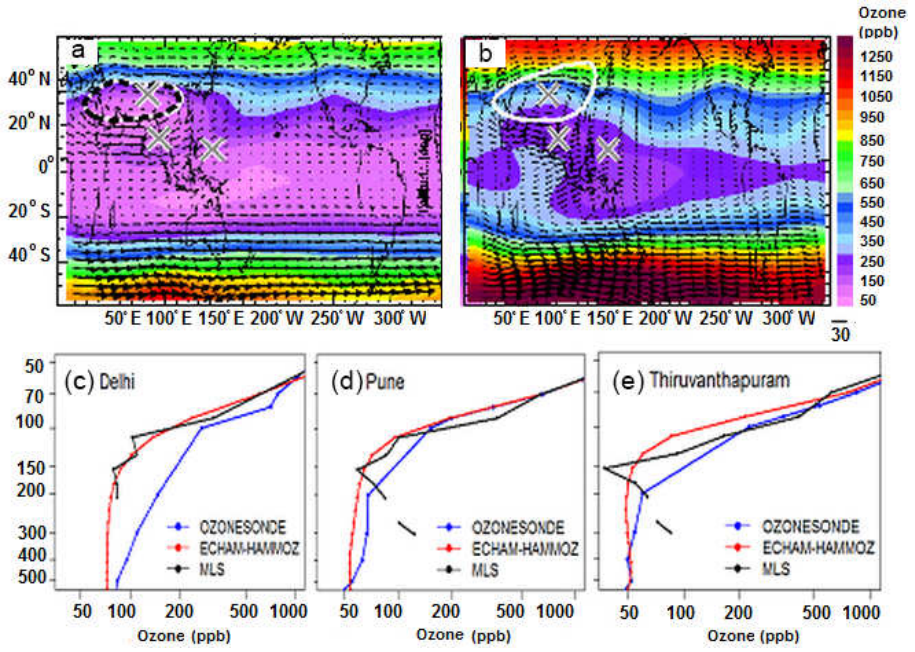

Figure 1. Distribution of ozone mixing ratio (ppb) during the monsoon season (June–September) obtained from **(a)** MLS observations at 100 hPa and **(b)** ECHAM5-HAMMOZ at 90 hPa. Black arrows indicate wind vectors, the black dashed contour shows the PV-gradient-based transport barrier of the anticyclone (calculated following Ploeger et al., 2015), and the white contour shows the 270 m geopotential height anomaly, corresponding to the anticyclone edge definition by Barret et al. (2016). Meteorological data show climatological July fields from **(a)** ERA-Interim reanalysis and **(b)** ECHAM5-HAMMOZ. The ECHAM5-HAMMOZ ozone distribution is smoothed using the MLS averaging kernel. Grey crosses highlight the regions of the Tibetan Plateau, Bay of Bengal, and South China Sea. Bottom panels show the vertical distribution of seasonal (June–September) mean ozone mixing ratios (ppb) from ozonesonde (2001–2009), MLS (2004–2013) and ECHAM5-HAMMOZ CTRL simulation at the **(c)** Delhi, **(d)** Pune, and **(e)** Thiruvananthpuram Indian stations.

to characterize the extent of the anticyclone are based either on potential vorticity on isentropic surfaces or on geopotential height on pressure surfaces. Here we apply both characterizations of the anticyclone and show the PV contour related to the maximum PV gradient on 380 K (calculated from ERA-Interim reanalysis following Ploeger et al., 2015), and the 270 m geopotential height anomaly as proposed by Barret et al. (2016). The close agreement of both methods shows that from a climatological point of view the two criteria yield a very similar picture of the anticyclonic circulation and the related trace gas confinement. Locally and at particular dates, however, differences may be larger with potential vorticity correlating better with confined trace gas anomalies than geopotential height (e.g. Garny and Randel, 2013; Ploeger et al., 2015). The spatial pattern of low ozone concentrations in the monsoon anticyclone is well simulated in the model. It is in good agreement with MLS (90–140 ppbv), MIPAS (80–120 ppbv), and SAGE II (< 150 ppbv) measurements (Kunze et al., 2010; Randel et al., 2001; Randel and Park, 2006; Park et al., 2007).

Vertical profiles of ozonesonde measurements (averaged for the monsoon season during 2001–2009) at Indian stations, Delhi (28.61° N, 77.23° E), Pune (18.52° N, 73.85° E), and Thiruvananthapuram (8.48° N, 76.95° E) are compared with MLS measurements and ECHAM5-HAMMOZ simulated ozone mixing ratios in Fig. 1c–e. ECHAM5-HAMMOZ simulations show good agreement with MLS data between 200 and 50 hPa at all three stations. Comparison of ozonesonde observations with the ECHAM5-HAMMOZ simulation shows reasonably good agreement at Pune compared to Delhi and Thiruvananthapuram, where there are some discrepancies. The simulated ozone mixing ratios are lower than ozonesonde measurements by 10–40 ppb between 500 and 90 hPa at Pune and by ∼ 70–90 ppb in the upper troposphere (500–150 hPa) at Delhi. At Thiruvananthapuram, while at altitudes below 375 hPa simulated ozone mixing ratios show good agreement with ozonesonde data, at the altitudes above 375 hPa simulated values are lower than observations by ∼ 20–70 ppb. The differences between model and ozonesonde data may be due to different grid sizes: the ECHAM5-HAMMOZ model grid size is ∼ 280 km, while balloon observations are within ∼ 30–180 km spatial range (balloon typically drifts ∼ 30–180 km horizontally). In addition, previous work comparing these model simulations with various aircraft observations during the monsoon season found a reasonable agreement for PAN, NO_x, HNO_3, and O_3 mixing ratios (Fadnavis et al., 2014).

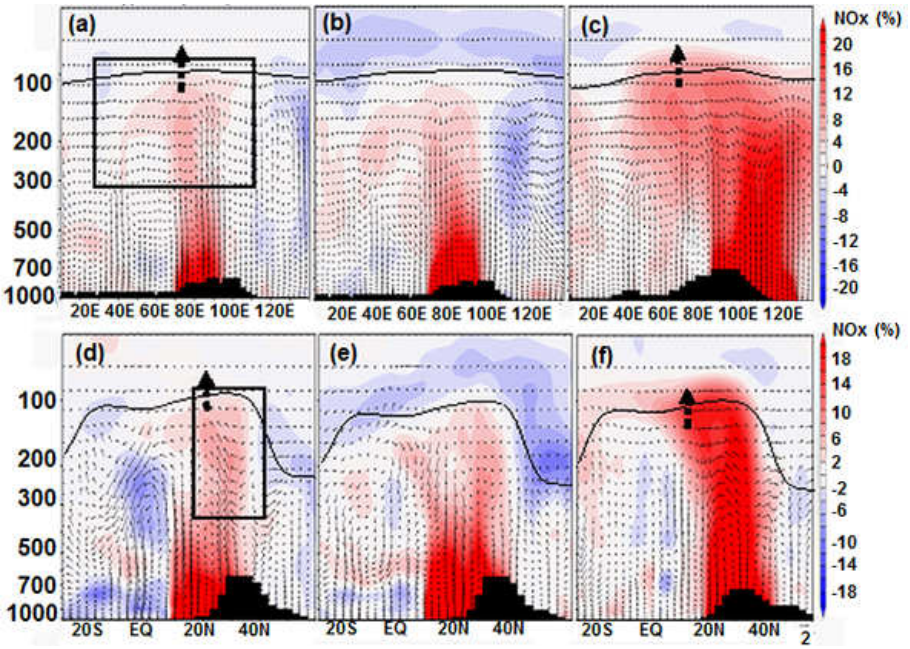

Figure 2. Longitude–pressure cross sections of percentage NO_x anomalies averaged for the monsoon season (June–September) obtained from **(a)** Ind38 (averaged over 8–35° N), **(b)** Ind73 (averaged over 8–35° N), and **(c)** Chin73 (averaged over 20–45° N) simulations. Latitude–pressure cross sections of percentage NO_x anomalies averaged for the monsoon season (June–September) obtained from **(d)** Ind38 (averaged over 70–90° E), **(e)** Ind73 (averaged over 70–90° E), and **(f)** Chin73 (averaged over 85–120° E) simulations. Black arrows indicate wind vectors (the vertical velocity field has been scaled by 300), the black line represents the tropopause, and the black dashed arrows indicate the cross-tropopause transport. The black boxes show the outline of the anticyclone.

3.2 Transport of enhanced NO_x emissions into the UTLS

Recent satellite observations and model simulations demonstrated the impact of convective transport of boundary layer pollution into the ASM anticyclone during the ASM season (Gettelman et al., 2004; Randel et al., 2010; Fadnavis et al., 2013, 2014, 2015). These pollutants are further transported across the tropopause as evident in satellite observations of e.g. water vapour (Bian et al., 2012), HCN (Randel et al., 2010), CO (Schoeberl et al., 2006), PAN (Fadnavis et al., 2014, 2015), and aerosols (Vernier et al., 2015; Fadnavis et al., 2013). To understand the influence of monsoon convection on the vertical distribution of NO_x we show zonal and meridional cross sections over India and China. Vertical distributions of NO_x averaged for the monsoon season over Indian latitudes (8–35° N) and Chinese latitudes (20–45° N) as obtained from CTRL simulations are shown in Fig. S3a and b respectively. These figures show elevated levels of NO_x extending from the surface to the upper troposphere over India and China. The wind vectors along with the distribution of cloud droplet number concentration (CDNC) and ice crystal number concentration (ICNC) (Fig. S4a–c) indicate strong convective transport from the Bay of Bengal (BOB), South China Sea, and southern slopes of Himalayas, which might lift the boundary layer NO_x to the upper troposphere.

During the monsoon season, the NO_x distribution in the UTLS is also influenced by lightning, in addition to transport from anthropogenic sources. Lightning activity during this season was found to be more pronounced in Asia, compared to the other monsoon regions such as North America, South America, and Africa (Ranalkar and Chaudhari, 2009; Penki and Kamra, 2013). In our simulations, we find that lightning produces 40–70 % of NO_x over northern India and BOB and 40–60 % over the Tibetan Plateau and western China region (Fig. S5).

Figure 2 shows the vertical distribution of anthropogenic NO_x anomalies obtained from the Ind38, Ind73, and Chin73 simulations, compared with the CTRL simulation. Ind38 simulation shows that the convective winds over the BOB (80–90° E) (Fig. 2a) and at the southern flank of the Himalayas (Fig. 2d) lift up the enhanced Indian NO_x emissions to the UT. Similarly the Chin73 simulation shows that the convective winds over the South China Sea (100–120° E) (Fig. 2c) and over the Himalayas (Fig. 2f) lift up the enhanced Chinese NO_x emissions to the UT. While most transport is mainly into the UT, parts of it also occur into the lower stratosphere, with cross-tropopause transport being particularly evident in the Chin73 simulation (Fig. 2c and f). Randel and Park (2006) and Randel et al. (2010) also reported that pollution transported by Asian monsoon convection enters the stratosphere. Our results are also in good agreement with

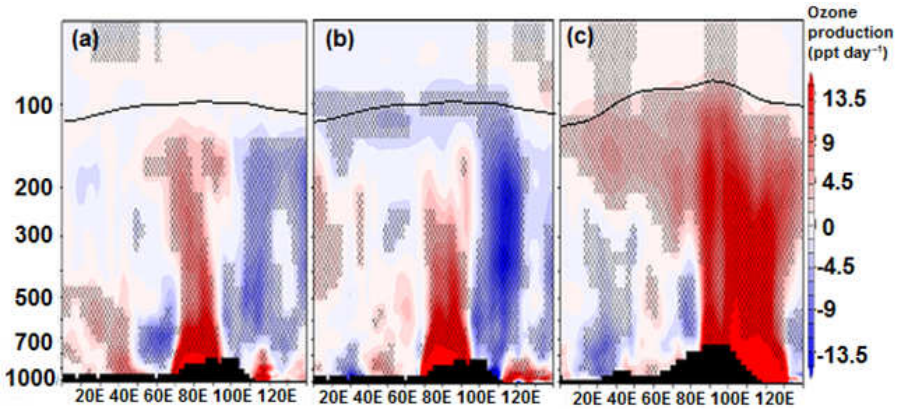

Figure 3. Longitude–pressure cross section of changes in net ozone production (ppt day^{-1}) due to enhanced NO_x with respect to the CTRL simulation, averaged for the monsoon season (June–September) obtained from **(a)** Ind38 (averaged over 8–35° N), **(b)** Ind73 (averaged over 8–35° N), and **(c)** Chin73 (over 20–45° N) simulations. The black line shows the tropopause while black hatched lines indicate 95 % confidence level.

previous studies indicating significant vertical transport due to strong monsoon convection from the southern slopes of Himalayas (Fu et al., 2006; Fadnavis et al., 2013, 2015) and the South China Sea (Park et al., 2009; Chen et al., 2012). In the upper troposphere, NO_x is transported over Iran and Saudi Arabia along the descending branch of the large scale monsoon circulation (Rodwell and Hoskins, 1995). However, the cross-tropopause transport is not present in the Ind73 simulation, where it is inhibited by the wind anomalies that show a descending branch over central India (∼ 20° N, 75° E) (Fig. 2b and e). These descending wind anomalies may also be related to the associated ozone radiative forcing and temperature changes, as discussed in Sect. 4.

3.3 Impact of enhanced anthropogenic NO_x on the tropospheric ozone distribution

We calculate the change in ozone production over India and China due to enhanced NO_x emissions in the Ind38, Ind73, and Chin73 simulations with respect to the CTRL simulation. Figure 3, showing longitude–pressure cross sections of net ozone production (ppt day^{-1}) changes, indicates that the majority of this additional ozone production occurs in the lower troposphere. At altitudes below 300 hPa, the ozone production and loss vary between −15 and 15 ppt day^{-1}. In the upper troposphere (300–150 hPa), the estimated amount of additional net ozone production in Ind38 and Ind73 simulation is 3–7 ppt day^{-1}, while in the Chin73 simulation it is ∼ 3–13 ppt day^{-1}. We also simulate ozone loss near the tropopause in the Ind73 simulation (Fig. 3b). We note that these ozone anomalies are not driven by lightning NO_x, as this is included in all simulations. It is interesting to understand ozone production over the highly populated Indo-Gangetic Plain and Tibetan Plateau region (these regions are marked in Fig. S4). A longitude–pressure cross section over this region show that ozone production over the Indo-Gangetic Plain and Tibetan Plateau in Ind73 is (20–25 ppt day^{-1}) is much larger than Ind38 (6–20 ppt day^{-1}) in the lower troposphere (Fig. S6).

Figure 4 shows the vertical distribution of ozone anomalies induced by enhanced anthropogenic NO_x emissions in the three perturbation experiments compared to the CTRL simulation, averaged over India and China. Although the air mass in the monsoon anticyclone is relatively poor in ozone (Fig. 1b), the elevated amounts of ozone anomalies in response to enhanced anthropogenic NO_x emissions are clearly seen in Fig. 4. This may be partially due to convective transport of enhanced-NO_x-emission-induced ozone anomalies produced in the lower troposphere and partially due to chemical ozone production from convectively transported boundary layer ozone precursors. Ozone anomalies are enhanced near 300–200 hPa over western Asia (40–60° E) (Fig. 4a–c), possibly due to the vertical convective transport of ozone anomalies and precursors and also from subsequent horizontal transport in the monsoon anticyclone (Barret et al., 2016).

Latitude–pressure cross sections of enhanced-NO_x-emission-induced ozone anomalies plotted in Fig. 4d and f illustrate how convection over the BOB, the southern slopes of the Himalayas and the South China Sea lifts the enhanced ozone anomalies from India and China into the upper troposphere. These ozone anomalies are also transported further across the tropopause and into the lower stratosphere, where ozone production is also driven by photolysis and NO_x anomalies.

In the Ind73 simulation, similarly to the NO_x anomaly distribution (Fig. 2b and e), the descending branch of circulation over central India also suppresses the vertical transport of ozone anomalies across the tropopause (Fig. 4b and e). This subsidence may be related to ozone heating rate changes, as there is significant increase in ozone production over the Indo-Gangetic Plain and Tibetan Plateau in the lower tro-

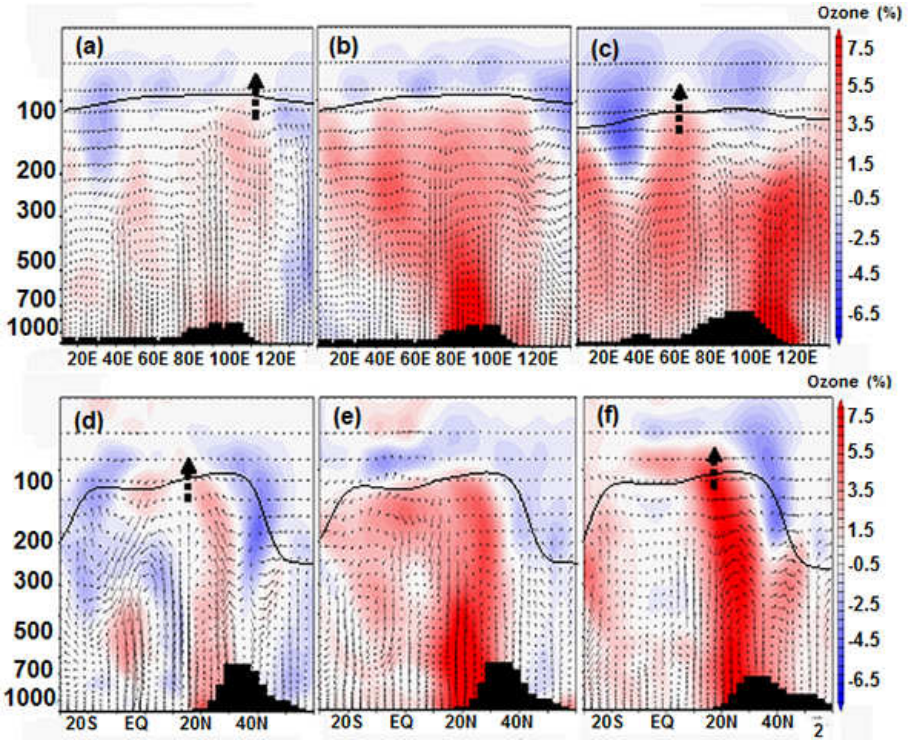

Figure 4. Longitude–pressure cross section of percentage ozone anomalies averaged for the monsoon season (June–September) obtained from **(a)** Ind38 (averaged over 8–35° N), **(b)** Ind73 (averaged over 8–35° N), and **(c)** Chin73 (averaged over 20–45° N) simulations. Latitude–pressure cross section of percentage ozone anomalies averaged for the monsoon season (June–September) obtained from **(d)** Ind38 (averaged over 70–90° E), **(e)** Ind73 (averaged over 70–90° E), and **(f)** Chin73 (averaged over 85–120° E) simulations. Black arrows indicate wind vectors. The vertical velocity field has been scaled by 300. The black line represents the tropopause, and the black dashed arrows indicate the cross-tropopause transport.

posphere due to enhanced anthropogenic NO_x emissions (Sect. 4).

3.4 Distribution of NO_x and ozone in the anticyclone

The distributions of NO_x and ozone anomalies in the monsoon anticyclone region in the Ind38, Ind73, and Chin73 simulations with respect to the CTRL simulation are shown in Fig. 5a–f. A maximum in the NO_x anomalies in the ASM anticyclone (60 to 120° E) is seen in all the simulations. NO_x anomalies are high at the eastern part of the monsoon anticyclone since convective injection into the anticyclone occurs mainly in that region (Fadnavis et al., 2013). Increase in NO_x anomalies in the Ind38 simulation is higher (Fig. 5a) than that in the Ind73 simulation (Fig. 5b), mainly due to descending motion over central India in the Ind73 simulation, as seen in the previous sections. In contrast to NO_x anomalies, ozone anomalies in Ind38 are lower than Ind73, especially in the north-eastern part of anticyclone. Satellite observations also show high ozone precursors and low ozone amounts in the anticyclone (Park et al., 2007; Barret et al., 2016). Similarly, the Chin73 simulation shows higher values of NO_x anomalies ($> 18\,\%$) and strong negative ozone anomalies ($\sim -8\,\%$) in the north-eastern region of the monsoon anticyclone (Fig. 5c and f). Figure 5 also shows that the tropical easterly jet transports NO_x and ozone (from India and China) to Saudi Arabia, Iran, and Iraq.

4 Discussion

To estimate the radiative impact of the simulated ozone changes, we use the offline version of the Edwards and Slingo (1996) radiative transfer model. Figure 6 shows the radiative forcing caused by the ozone changes in each of the three sensitivity simulations compared to the CTRL simulation. The overall increase in tropospheric ozone (see Fig. 4) has a warming effect on climate, with the regional average radiative forcing in the monsoon anticyclone (15–40° N, 60–120° E) estimated at 16.3, 69.9, and 78.5 mW m^{-2} in the Ind38, Ind73, and Chin73 simulations respectively.

We also investigate the impact on the atmospheric heating rates caused by the ozone changes. Figure 7 shows the zonal mean heating rate anomalies for the Ind38, Ind73, and Chin73 simulations compared to the CTRL simulation. These three simulations show positive and negative heating rates anomalies between 400 and 200 hPa. How-

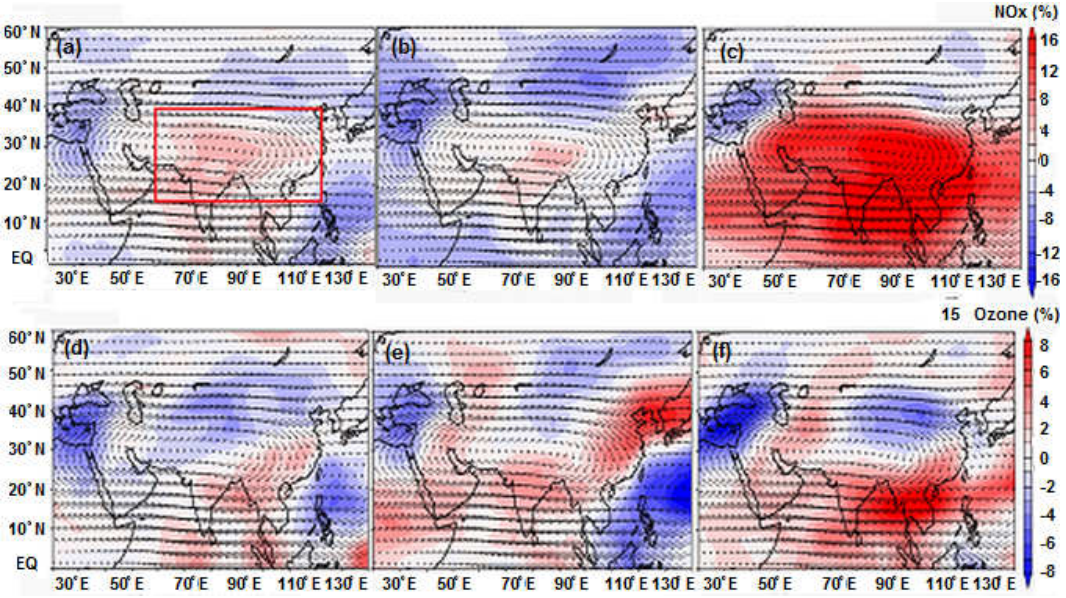

Figure 5. Latitude–longitude cross section of percentage NO_x anomalies averaged for the monsoon season (June–September) at 110 hPa obtained from **(a)** Ind38, **(b)** Ind73, and **(c)** Chin73 simulations. **(d–f)** show the same but for percentage ozone anomalies at 110 hPa for the **(d)** Ind38, **(e)** Ind73, and **(f)** Chin73 simulations. Black arrows indicate horizontal winds at 110 hPa. The red box in **(a)** indicates the ASM anticyclone region used to compute the associated radiative forcing regional average.

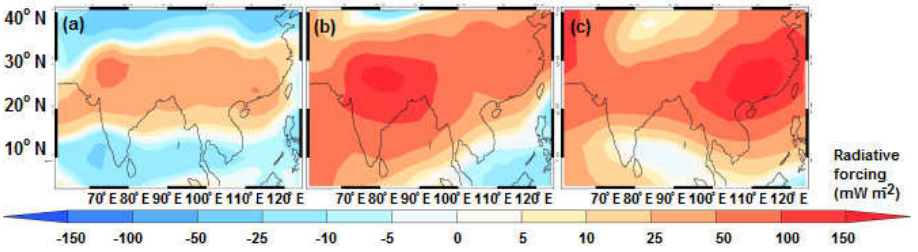

Figure 6. Latitude–longitude distribution of changes in ozone radiative forcing (in mW m^{-2}) for the **(a)** Ind38, **(b)** Ind73, and **(c)** Chin73 perturbed simulations, compared to the CTRL simulation.

ever, in the UTLS (200–50 hPa) ozone heating rates are negative over Indo-Gangetic Plain (20–30° N) and Tibetan Plateau (30–40° N) region. In Ind73 simulation, ozone heating rate anomalies are positive in the lower troposphere over the Indo-Gangetic Plain (1000–750 hPa) and Tibetan Plateau (600–400 hPa). This may be due to large amount of ozone production in the lower troposphere over these regions (Fig. S6). This heating may produce changes in the circulation leading to ascending motion over the Tibetan Plateau and a descending branch over central India (∼ 20° N), i.e. a reversal of monsoon Hadley circulation (Fig. 9b).

Figure 8 shows latitude–pressure cross section of temperature anomalies (K) obtained from Ind38, Ind73, and Chin73 simulations. Ind38 and Chin73 simulations show anomalous warming in the upper troposphere over the Tibetan Plateau while it is subdued in the Ind73 simulation. Upper-tropospheric warming over the Tibetan Plateau is one of the key factors responsible for the ASM circulation (Yanai et al., 1992; Meehl, 1994; Li and Yanai, 1996; Wu and Zhang, 1998). Flohn (1960) suggested that upper-tropospheric warming over the Tibetan Plateau leads to increased Indian summer monsoon rainfall by enhancing the cross-equatorial circulation that brings rainfall to India (Rajagopalan and Molnar, 2013; Vinoj et al., 2014). Goswami et al. (1999) also reported that there is a strong correlation between Hadley circulation and monsoon precipitation.

Figure 9a–c depict the change in monsoon Hadley cell circulation (averaged over 70–100° E) obtained from the difference in the Ind38, Ind73, and Chin73 and CTRL simulations. The Ind38 and Chin 73 simulations show a strengthening of the Hadley circulation: a strong ascending branch of the Hadley cell around 10–20° N (Fig. 9a), whereas the tilted descending branch of Hadley cell is seen over 20° N in the Ind73 simulation (Fig. 9b). In Ind73 simulation ozone heating rates are positive and negative in the vertical direction near ∼ 20° N (Fig. 7b), which might have attributed tilted de-

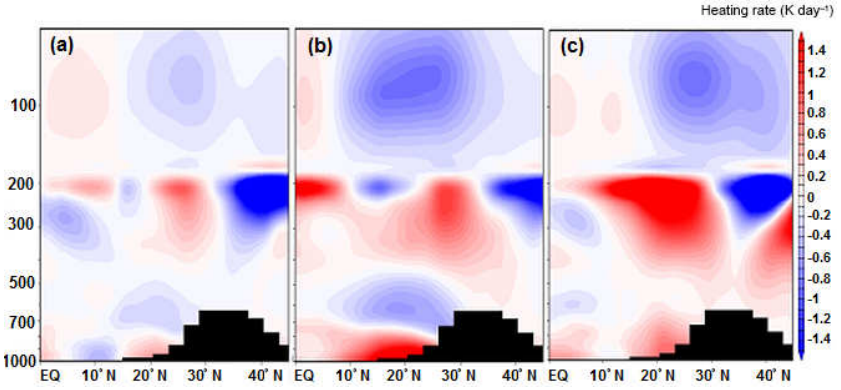

Figure 7. Latitude–pressure distribution of ozone heating rate changes (in K day^{-1}) for the **(a)** Ind38 (averaged over 70–100° E), **(b)** Ind73 (averaged 70–100° E), and **(c)** Chin73 (averaged over 70–100° E) perturbed simulations, compared to the CTRL simulation.

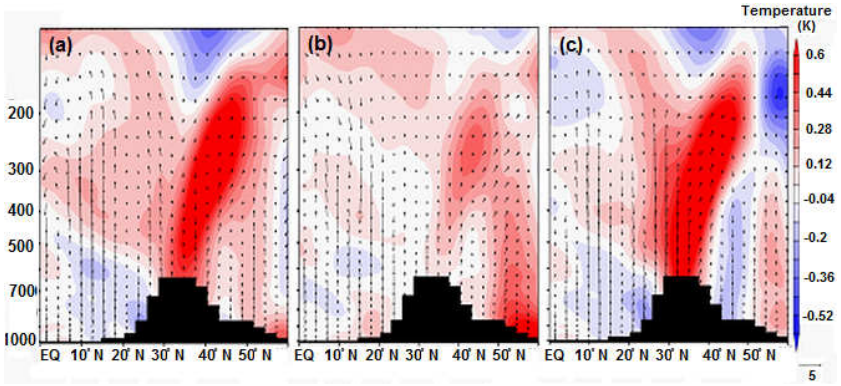

Figure 8. Latitude–pressure cross section of temperature anomalies (K) averaged for the monsoon season (June–September) and over 70–100° E obtained from **(a)** Ind38-CTRL, **(b)** Ind73-CTRL, and **(c)** Chin73-CTRL simulations. Black arrows indicate wind vectors (the vertical velocity field has been scaled by 300).

scending branch of Hadley cell. Consequently, precipitation anomalies over the Indian region (70–90° E, 8–35° N) are positive (0.3 to 0.9 mm day^{-1}) in the Ind38 and Chin73 simulations (Fig. 9d and f), whereas they are negative in the Ind73 simulation (-0.3 to -0.6 mm day^{-1}) (Fig. 9e). In the upper troposphere (250–100 hPa), Ind73 simulation shows subsidence while Chin73 simulation shows ascending motion at these levels over the Indian region. Upper-tropospheric subsidence in Ind73 simulation might have contributed to the weak positive and negative precipitation anomalies over the northern Indian region (Fig. 9e). The Chin73 simulation shows subsidence near 22° N below 200 hPa and ascending motion above it. The Chin73 simulation shows ascending motion near 12° N rising up to 110 hPa, which leads to positive precipitation anomalies over the Indian peninsula.

Thus, enhanced Indian (Ind38) and Chinese (Chin73) NO_x emissions increase warming over the Tibetan Plateau and enhance precipitation over India via a strengthening of the monsoon Hadley circulation. Remarkably, a further increase of NO_x emissions over India (Ind73) leads to high amounts of ozone in the lower troposphere over the Indo-Gangetic Plain and Tibetan Plateau. The related ozone heating induces a reversal of the monsoon Hadley circulation, thereby resulting in negative precipitation anomalies.

5 Conclusions

In this paper we investigate the potential impacts of enhanced anthropogenic NO_x emissions on ozone production and distribution during the monsoon season using the state-of-the-art ECHAM5-HAMMOZ model simulations. We performed sensitivity experiments for anthropogenic NO_x enhancements of 38 % over India (Ind38 simulation) and 73 % over China (Chin73 simulation) in accordance with recently observed trends of 3.8 % per year over India and 7.3 % per year over China (Ghude et al., 2013; Schneider and van der A, 2012). In another experiment, anthropogenic NO_x emissions over India are increased by 73 %, equal to Chinese emissions (Ind73 simulation).

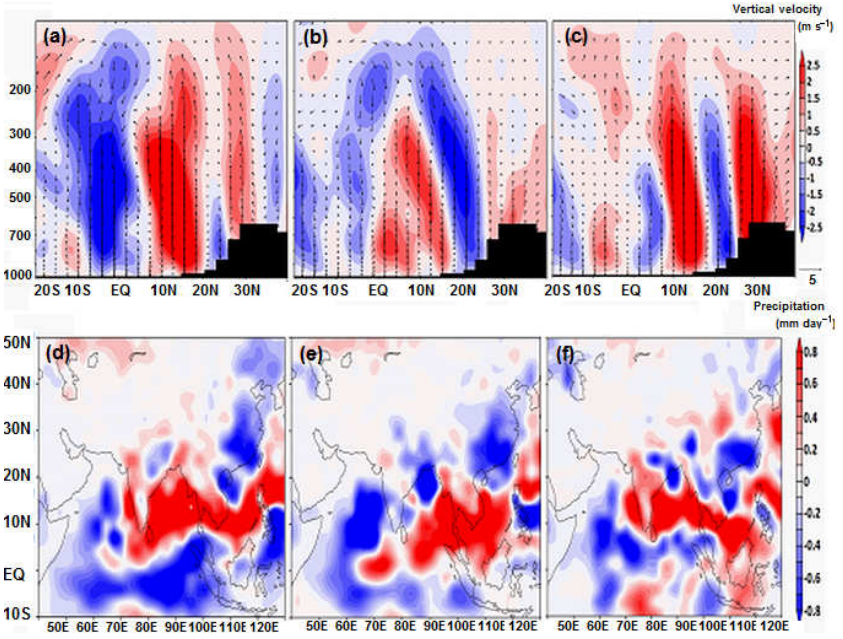

Figure 9. Difference in the meridional circulation due to enhanced NO_x emissions averaged for the monsoon season (June–September) and over 70–100° E for **(a)** Ind38-CTRL, **(b)** Ind73-CTRL, and **(c)** Chin73-CTRL simulations. Shaded contours indicate the anomalies in vertical velocity ($m\,s^{-1}$). The vertical velocity field has been scaled by 300. Precipitation anomalies ($mm\,day^{-1}$) averaged for the monsoon season (June–September) obtained from **(d)** India38-CTRL, **(e)** Ind73-CTRL, and **(f)** Chin73-CTRL simulations.

These simulations show that an increase in anthropogenic NO_x emissions (over India and China) increases ozone production in the lower and mid-troposphere. The monsoon convection at the southern flank of the Himalayas (80–90° E) and over the BOB lifts up the NO_x and ozone anomalies from India across the tropopause into the lower stratosphere (Figs. 2a–c, 4a–b and S4). Cross-tropopause transport also occurs over China due to convection over the South China Sea.

Increase in NO_x emissions in the Ind38, Ind73, and Chin73 simulations leads to increase in ozone radiative forcings, in the anticyclone (15–40° N, 60–120° E) of 16.25, 69.88, and 78.51 $mW\,m^{-2}$ in the Ind38, Ind73, and Chin73 simulations respectively. Enhanced ozone production (Ind38 and Chin73 simulations) increases ozone heating rates, which cause anomalous warming over the Tibetan Plateau. Further increase in NO_x emissions over the India region (Ind73 simulation) produces anomalous heating in the lower troposphere over the Indo-Gangetic Plain and Tibetan Plateau. This warming elicits the reversal of the monsoon Hadley cell circulation. The descending branch of the monsoon Hadley circulation over the central India impedes vertical transport of ozone and NO_x anomalies.

In the Ind38 and Chin73 simulations, anomalous warming over the Tibetan Plateau results in a strengthening of the monsoon Hadley circulation over India and elicits positive precipitation (0.3 to 0.9 $mm\,day^{-1}$) anomalies over India. However, in Ind73 simulations the reversal of the Hadley circulation and the concurrent subdued warming in the upper troposphere over the Tibetan Plateau results in negative precipitation anomalies (−0.3 to −0.6 $mm\,day^{-1}$) over India.

6 Data availability

We have provided reference for the data we used. We have used satellite data, which are freely available. We have provided a link (http://mls.jpl.nasa.gov/) in Sect. 2.1 from which data can be accessed. We have also used RETRO emission data for the model simulations. These data are freely available at http://eccad.sedoo.fr/, as mentioned in Sect. 2.2.

The Supplement related to this article is available online at doi:10.5194/acp-17-1297-2017-supplement.

Competing interests. The authors declare that they have no conflict of interest.

Acknowledgements. Suvarna Fadnavis and Chaitri Roy acknowledges with gratitude R. Krishnan, Director of IITM, for his encouragement during the course of this study. We also thank two anonymous reviewers for their valuable suggestions for improvement of this paper. The authors acknowledge the High Power Computing Centre (HPC) in IITM, Pune, India, for providing

computer resources. Part of the research leading to these results has received funding from the European Community's Seventh Framework Programme (FP7/2007-2013) in the frame of the StratoClim project under grant agreement number 603557. Felix Ploeger was supported by the Helmholtz Young Investigators Group grant A-SPECi (VH-NG-1128).

Edited by: M. Dameris
Reviewed by: F. Khosrawi and one anonymous referee

References

Abad, G. G., Allen, N. D. C., Bernath, P. F., Boone, C. D., McLeod, S. D., Manney, G. L., Toon, G. C., Carouge, C., Wang, Y., Wu, S., Barkley, M. P., Palmer, P. I., Xiao, Y., and Fu, T. M.: Ethane, ethyne and carbon monoxide concentrations in the upper troposphere and lower stratosphere from ACE and GEOS-Chem: a comparison study, Atmos. Chem. Phys., 11, 9927–9941, doi:10.5194/acp-11-9927-2011, 2011.

Abhik, S., Mukhopadhyay, P., and Goswami, B. N., Evaluation of mean and intraseasonal variability of Indian summer monsoon simulation in ECHAM5: identification of possible source of bias, Clim. Dynam., 43, 389–406, 2014.

Barret, B., Sauvage, B., Bennouna, Y., and Le Flochmoen, E.: Upper-tropospheric CO and O_3 budget during the Asian summer monsoon, Atmos. Chem. Phys., 16, 9129–9147, doi:10.5194/acp-16-9129-2016, 2016.

Bekki, S., Rap, A., Poulain, V., Dhomse, S., Marchand, M., Lefevre, F., Forster, P. M., Szopa, S., and Chipperfield, M. P.: Climate impact of stratospheric ozone recovery, Geophys. Res. Lett., 40, 2796–2800, doi:10.1002/grl.50358, 2013.

Bian, J., Pan, L. L., Paulik, L., Vömel, H., Chen, H., and Lu, D.: In situ water vapor and ozone measurements in Lhasa and Kunming during the Asian summer monsoon, Geophys. Res. Lett., 39, L19808, doi:10.1029/2012GL052996, 2012.

Braesicke, P., Smith, O. J., Telford, P., and Pyle, J. A.: Ozone concentration changes in the Asian summer monsoon anticyclone and lower stratospheric water vapour: An idealised model study, Geophys. Res. Lett., 38, L03810, doi:10.1029/2010GL046228, 2011.

Chatani, S., Amann, M., Goel, A., Hao, J., Klimont, Z., Kumar, A., Mishra, A., Sharma, S., Wang, S. X., Wang, Y. X., and Zhao, B.: Photochemical roles of rapid economic growth and potential abatement strategies on tropospheric ozone over South and East Asia in 2030, Atmos. Chem. Phys., 14, 9259–9277, doi:10.5194/acp-14-9259-2014, 2014.

Chen, B., Xu, X. D., Yang, S., and Zhao, T. L.: Climatological perspectives of air transport from atmospheric boundary layer to tropopause layer over Asian monsoon regions during boreal summer inferred from Lagrangian approach, Atmos. Chem. Phys., 12, 5827–5839, doi:10.5194/acp-12-5827-2012, 2012.

Dentener, F., Kinne, S., Bond, T., Boucher, O., Cofala, J., Generoso, S., Ginoux, P., Gong, S., Hoelzemann, J. J., Ito, A., Marelli, L., Penner, J. E., Putaud, J.-P., Textor, C., Schulz, M., van der Werf, G. R., and Wilson, J.: Emissions of primary aerosol and precursor gases in the years 2000 and 1750 prescribed data-sets for AeroCom, Atmos. Chem. Phys., 6, 4321–4344, doi:10.5194/acp-6-4321-2006, 2006.

Druyan, L. M., Fulakeza, M., and Lonergan, P.: The impact of vertical resolution on regional model simulation of the west African summer monsoon, Int. J. Climatol, 28, 1293–1314, doi:10.1002/joc.1636, 2008.

Edwards, J. M. and Slingo, A.: Studies with a flexible new radiation code. 1. Choosing a configuration for a large-scale model, Q. J. Roy. Meteorol. Soc., 122, 689–719, doi:10.1002/qj.49712253107, 1996.

Fadnavis, S., Semeniuk, K., Pozzoli, L., Schultz, M. G., Ghude, S. D., Das, S., and Kakatkar, R.: Transport of aerosols into the UTLS and their impact on the Asian monsoon region as seen in a global model simulation, Atmos. Chem. Phys., 13, 8771–8786, doi:10.5194/acp-13-8771-2013, 2013.

Fadnavis, S., Schultz, M. G., Semeniuk, K., Mahajan, A. S., Pozzoli, L., Sonbawne, S., Ghude, S. D., Kiefer, M., and Eckert, E.: Trends in peroxyacetyl nitrate (PAN) in the upper troposphere and lower stratosphere over southern Asia during the summer monsoon season: regional impacts, Atmos. Chem. Phys., 14, 12725–12743, doi:10.5194/acp-14-12725-2014, 2014.

Fadnavis, S., Semeniuk, K., Schultz, M. G., Kiefer, M., Mahajan, A., Pozzoli, L., and Sonbawane, S.: Transport pathways of peroxyacetyl nitrate in the upper troposphere and lower stratosphere from different monsoon systems during the summer monsoon season, Atmos. Chem. Phys., 15, 11477–11499, doi:10.5194/acp-15-11477-2015, 2015.

Fiore, A. M., Horowitz, L. W., Purves, D. W., Levy II, H., Evans, M. J., Wang, Y., Li, Q., and Yantosca, R. M.: Evaluating the contribution of changes in isoprene emissions to surface ozone trends over the eastern United States, J. Geophys. Res., 110, D12303, doi:10.1029/2004JD005485, 2005.

Flohn, H.: Recent investigations on the mechanism of the "Summer Monsoon" of Southern and Eastern Asia, Symposium on "Monsoons of the world", 19–21 February 1958, New Delhi, India, 75–88, 1960.

Forster, F., Piers, M., and Shine, K. P.: Radiative forcing and temperature trends from stratospheric ozone changes, J. Geophys. Res., 102, 10841–10855, 1997.

Froidevaux, L., Livesey, N. J., Read, W. G., Jiang, Y. B., Jimenez, C. J., Filipiak, M. J., Schwartz, M. J., Santee, M. L., Pumphrey, H. C., Jiang, J. H., Wu, D. L., Manney, G. L., Drouin, B. J., Waters, J. W., Fetzer, E. J., Bernath, P. F., Boone, C. D., Walker, K. A., Jucks, K. W., Toon, G. C., Margitan, J. J., Sen, B., Webster, C. R., Christensen, L. E., Elkins, J. W., Atlas, E., Ueb, R. A., and Hendershot, R.: Early validation analyses of atmospheric profiles from EOS MLS on the Aura satellite, IEEE T. Geosci. Remote, 44, 1106–1121, doi:10.1109/TGRS.2006.864366, 2006.

Fu, R., Hu, Y. L., Wright, J. S., Jiang, J. H., Dickinson, R. E., Chen, M. X., Filipiak, M., Read, W. G., Waters, J. W., and Wu, D. L.: Short circuit of water vapor and polluted air to the global stratosphere by convective transport over the Tibetan Plateau, P. Natl. Acad. Sci. USA, 103, 5664–5669, doi:10.1073/pnas.0601584103, 2006.

Ganzeveld, L. and Lelieveld, J.: Dry deposition parameterization in a chemistry general circulation model and its influence on the distribution of reactive trace gases, J. Geophys. Res., 100, 20999–21012, doi:10.1029/95JD02266, 1995.

Garny, H. and Randel, W. J.: Dynamic variability of the Asian monsoon anticyclone observed in potential vorticity and correlations

with tracer distributions, J. Geophys. Res.-Atmos., 118, 13421–13433, doi:10.1002/2013JD020908, 2013.

Gettelman, A., Kinnison, D. E., Dunkerton, T. J., and Brasseur, G. P.: Impact of monsoon circulations on the upper troposphere and lower stratosphere, J. Geophys. Res., 109, D22101, doi:10.1029/2004jd004878, 2004.

Ghude, S. D., Kulkarni, S. H., Jena, C., Pfister, G. G., Beig, G., Fadnavis, S., and van der A, R. J.: Application of satellite observations for identifying regions of dominant sources of nitrogen oxides over the Indian Subcontinent, J. Geophys. Res., 118, 1–15, doi:10.1029/2012JD017811, 2013.

Goswami, B. N., Krishnamurthy, V., and Annamalai, H.: A broad-scale circulation index for the interannual variability of the Indian summer monsoon. Q. J. Roy. Meteorol. Soc., 125, 611–633, doi:10.1002/qj.49712555412, 1999.

Grewe, V., Brunner, D., Dameris, M., Grenfell, J. L., Hein, R., Shindell, D., and Staehelin, J.: Origin and Variability of Upper Tropospheric Nitrogen Oxides and Ozone at Northern Mid-Latitudes, Atmos. Environ., 35, 3421–3433, doi:10.1016/S1352-2310(01)00134-0, 2001.

Gu, D., Wang, Y., Smeltzer, C., and Boersma, K. F.: Anthropogenic emissions of NO_x over China: Reconciling the difference of inverse modeling results using GOME-2 and OMI measurements, J. Geophys. Res.-Atmos., 119, 7732–7740, doi:10.1002/2014JD021644, 2014.

Hilboll, A., Richter, A., and Burrows, J. P.: Long-term changes of tropospheric NO_2 over megacities derived from multiple satellite instruments, Atmos. Chem. Phys., 13, 4145–4169, doi:10.5194/acp-13-4145-2013, 2013.

Horowitz, L. W., Walters, S., Mauzerall, D. L., Emmons, L. K., Rasch, P. J., Granier, C., Tie, X., Lamarque, J., Schultz, M. G.,Tyndall, G. S., Orlando, J. J., and Brasseur, G. P.: A global simulation of tropospheric ozone and related tracers, Description and evaluation of MOZART, version 2, J. Geophys. Res., 108, 4784, doi:10.1029/2002JD002853, 2003.

Jacob, D. J., Logan, J. A., and Murti, P. P.: Effect of rising Asian emissions on surface ozone in the United States, Geophys. Res. Lett., 26, 2175–2178, doi:10.1029/1999GL900450, 1999.

Kärcher, B. and Lohmann, U.: A parameterization of cirrus cloud formation: Homogeneous freezing of supercooled aerosols, J. Geophy. Res., 107, 4010, doi:10.1029/2001JD000470, 2002.

Konopka, P., Grooß, J.-U., Günther, G., Ploeger, F., Pommrich, R., Müller, R., and Livesey, N.: Annual cycle of ozone at and above the tropical tropopause: observations versus simulations with the Chemical Lagrangian Model of the Stratosphere (CLaMS), Atmos. Chem. Phys., 10, 121–132, doi:10.5194/acp-10-121-2010, 2010.

Kunze, M., Braesicke, P., Langematz, U., Stiller, G., Bekki, S., Brühl, C., Chipperfield, M., Dameris, M., Garcia, R., and Giorgetta, M.: Influences of the Indian summer monsoon on water vapor and ozone concentrations in the UTLS as simulated by chemistry-climate models, J. Climate, 23, 3525–3544, doi:10.1175/2010JCLI3280.1, 2010.

Lacis, A., Donald Wuebbles, J., and Logan, J. A.: Radiative Forcing of climate by Changes in the Vertical Distribution of Ozone, J. Geophys. Res., 95, 9971–9981, doi:10.1029/JD095iD07p09971, 1990.

Lawrence, M. G.: Atmospheric science: Asia under a high-level brown cloud, Nat. Geosci., 4, 352–353, doi:10.1038/ngeo1166, 2011.

Lei, W., Zhang, R., Tie, X., and Hess, P.: Chemical characterization of ozone formation in the Houston-Galveston area, J. Geophys. Res., 109, D12301, doi:10.1029/2003JD004219, 2004.

Li, C. and Yanai, M.: The onset and interannual variability of the Asian summer monsoon in relation to land–sea thermal contrast, J. Climate, 9, 358–375, doi:10.1175/1520-0442(1996)009<0358:TOAIVO>2.0.CO;2, 1996.

Li, Q., Jiang, J. H., Wu, D. L., Read, W. G., Livesey, N. J., Waters, J. W., Zhang, Y., Wang, B., Filipiak, M. J., Davis, C. P., Turquety, S., Wu, S., Park, R. J., Yantosca, R. M., and Jacob, D. J.: Convective outflow of south Asian pollution: a global CTM simulation compared with EOS MLS observations, Geophys. Res. Lett., 32, L14826, doi:10.1029/2005GL022762, 2005.

Livesey, N. J., Read, W. G., Filipiak, M. J., Froidevaux, L., Harwood, R. S., Jiang, J. H., Jimenez, C., Pickett, H. M., Pumphrey, H. C., Santee, M. L., Schwartz, M. J., Waters, J. W., and Wu, D. L.: EOS MLS Version 1.5 Level 2 data quality and description document, JPL, California, 2005.

Livesey, N. J., Read, W. G., Froideveaux, L., Lambert, A., Manney, G. L., Pumphrey, H. C., Santee, M. L., Schwartz, M. J., Wang, S., Cofield, R. E., Cuddy, D. T., Fuller, R. A., Jarnot, R. F., Jiang, J. H., Knosp, B. W., Stek, P. C., Wagner, P. A., and Wu, D. L.: Version 3.3 Level 2 data quality and description document, Tech. Rep. JPL D-33509, Jet Propulsion Laboratory, available at: http://mls.jpl.nasa.gov (last access: 17 August 2015), 2011.

Lohmann, U., Feichter, J., Chuang, C. C., and Penner, J. E.: Predicting the number of cloud droplets in the ECHAM GCM, J. Geophys. Res., 104, 9169–9198, 1999.

Meehl, G. A.: Coupled land-ocean-atmosphere processes and South Asian monsoon variability, Science, 266, 263–267, doi:10.1126/science.266.5183.263, 1994.

Myhre, G., Shindell, D., Bréon, F.-M., Collins, W., Fuglestvedt, J., Huang, J., Koch, D., Lamarque, J.-F., Lee, D., Mendoza, B., Nakajima, T., Robock, A., Stephens, G., Takemura, T., and Zhang, H.: Anthropogenic and Natural Radiative Forcing, in: Climate Change 2013: The Physical Science Basis, Contribution of Working Group I to the Fifth Assessment Report of the Intergovernmental Panel on Climate Change, edited by: Stocker, T. F., Qin, D., Plattner, G.-K., Tignor, M., Allen, S. K., Boschung, J., Nauels, A., Xia, Y., Bex, V., and Midgley, P. M., Cambridge University Press, Cambridge, UK and New York, NY, USA, 659–740, 2013.

Park, M., Randel, W. J., Kinnison, D. E., Garcia, R. R., and Choi, W.: Seasonal variation of methane, water vapour, and nitrogen oxides near the tropopause: Satellite observations and model simulations, J. Geophys. Res., 109, D03302, doi:10.1029/2003JD003706, 2004.

Park, M., Randel, W. J., Gettelman, A., Massie, S. T., and Jiang, J. H.: Transport above the Asian summer monsoon anticyclone inferred from Aura Microwave Limb Sounder tracers, J. Geophys. Res., 112, D16309, doi:10.1029/2006jd008294, 2007.

Park, M., Randel, W. J., Emmons, L. K., Bernath, P. F., Walker, K. A., and Boone, C. D.: Chemical isolation in the Asian monsoon anticyclone observed in Atmospheric Chemistry Experiment (ACE-FTS) data, Atmos. Chem. Phys., 8, 757–764, doi:10.5194/acp-8-757-2008, 2008.

Park, M., Randel, W. J., Emmons, L. K., and Livesey, N. J.: Transport pathways of carbon monoxide in the Asian summer monsoon diagnosed from Model of Ozone and Related Tracers (MOZART), J. Geophys. Res., 114, D08303, doi:10.1029/2008jd010621, 2009.

Penki, R. K. and Kamra, A. K.: Lightning distribution with respect to the monsoon trough position during the Indian summer monsoon season, J. Geophys. Res., 118, 4780–4787, doi:10.1002/jgrd.50382, 2013.

Ploeger, F., Gottschling, C., Griessbach, S., Grooß, J.-U., Guenther, G., Konopka, P., Müller, R., Riese, M., Stroh, F., Tao, M., Ungermann, J., Vogel, B., and von Hobe, M.: A potential vorticity-based determination of the transport barrier in the Asian summer monsoon anticyclone, Atmos. Chem. Phys., 15, 13145–13159, doi:10.5194/acp-15-13145-2015, 2015.

Pozzoli, L., Bey, I., Rast, J. S., Schultz, M. G., Stier, P., and Feichter, J.: Trace gas and aerosol interactions in the fully coupled model of aerosol-chemistry-climate ECHAM5-HAMMOZ: 1. Model description and insights from the spring 2001 TRACE-P experiment, J. Geophys. Res., 113, D07308, doi:10.1029/2007JD009007, 2008a.

Pozzoli, L., Bey, I., Rast, J. S., Schultz, M. G., Stier, P., and Feichter, J.: Trace gas and aerosol interactions in the fully coupled model of aerosol-chemistry-climate ECHAM5-HAMMOZ: 2. Impact of heterogeneous chemistry on the global aerosol distributions, J. Geophys. Res., 113, D07309, doi:10.1029/2007JD009008, 2008b.

Pozzoli, L., Janssens-Maenhout, G., Diehl, T., Bey, I., Schultz, M. G., Feichter, J., Vignati, E., and Dentener, F.: Re-analysis of tropospheric sulfate aerosol and ozone for the period 1980–2005 using the aerosol-chemistry-climate model ECHAM5-HAMMOZ, Atmos. Chem. Phys., 11, 9563–9594, doi:10.5194/acp-11-9563-2011, 2011.

Rajagopalan, B. and Molnar, P.: Signatures of Tibetan Plateau heating on Indian summer monsoon rainfall variability, J. Geophys. Res.-Atmos., 118, 1170–1178, doi:10.1002/jgrd.50124, 2013.

Rajeevan, M., Bhate, J., Kale, J. D., and Lal, B.: Development of High Resolution Daily Gridded Rainfall Data for the Indian Region, Met. Monograph Climatology No. 22/2005, National Climate Centre India Meteorological Department, Pune, India, 2005.

Ranalkar, M. R. and Chaudhari, H. S.: Seasonal variation of lightning activity over the Indian subcontinent, Meteorol. Atmos. Phys., 104, 125–134, doi:10.1007/s00703-009-0026-7, 2009.

Randel, W. J. and Park, M.: Deep convective influence on the Asian summer monsoon anticyclone and associated tracer variability observed with Atmospheric Infrared Sounder (AIRS), J. Geophys. Res., 111, D12314, doi:10.1029/2005JD006490, 2006.

Randel, W. J., Wu, F., Gettelman, A., Russell, J. M., Jawodny, J. M., and Oltmans, S. J.: Seasonal variation of water vapor in the lower stratosphere observed in Halogen Occultation Experiment data, J. Geophys. Res., 106, 14313–14325, doi:10.1029/2001JD900048, 2001.

Randel, W. J., Park, M., Emmons, L., Kinnison, D., Bernath, P., Kaley Walker, A., Boone, C., and Pumphrey, H.: Asian Monsoon Transport of Pollution to the Stratosphere, Science, 328, 611–613, doi:10.1126/science.1182274, 2010.

Rap, A., Richards, N. A. D., Forster, P. M., Monks, S., Arnold, S. R., and Chipperfield, M.: Satellite constraint on the tropospheric ozone radiative effect, Geophys. Res. Lett., 42, 5074–5081, doi:10.1002/2015GL064037, 2015.

Revell, L. E., Tummon, F., Stenke, A., Sukhodolov, T., Coulon, A., Rozanov, E., Garny, H., Grewe, V., and Peter, T.: Drivers of the tropospheric ozone budget throughout the 21st century under the medium-high climate scenario RCP6.0, Atmos. Chem. Phys., 15, 5887–5902, doi:10.5194/acp-15-5887-2015, 2015.

Richter, A., John Burrows, P., Hendrik, N., Granier, C., and Niemeier, U.: Increase in tropospheric nitrogen dioxide over China observed from space, Nature, 437, 129–132, doi:10.1038/nature04092, 2005.

Riese, M., Ploeger, F., Rap, A., Vogel, B., Konopka, P., Dameris, M., and Forster, P.: Impact of uncertainties in atmospheric mixing on simulated UTLS composition and related radiative effects, J. Geophys. Res.-Atmos., 117, D16305, doi:10.1029/2012JD017751, 2012.

Rodwell, M. J. and Hoskins, B. J.: Monsoons and the dynamics of deserts, Q. J. Roy. Meteorol. Soc., 122, 1385–1404, doi:10.1002/qj.49712253408, 1995.

Roeckner, E., Bauml, G., Bonaventura, L., Brokopf, R., Esch, M., Giorgetta, M., Hagemann, S., Kirchner, I., Kornblueh, L., Manzini, E., Rhodin, A., Schlese, U., Schulzweida, U., and Tompkins, A.: The atmospehric general circulation model ECHAM5: Part 1, Tech. Rep. 349, Max Planck Institute for Meteorology, Hamburg, 2003.

Sander, S. P., Finlayson-Pitts, B. J., Friedl, R. R., Golden, D. M., Huie, R. E., Keller-Rudek, H., Kolb, C. E., Kurylo, M. J., Molina, M. J., Moortgat, G. K., Orkin, V. L., Ravishankara, A. R., and Wine, P. H.: Chemical Kinetics and Photochemical Data for Use in Atmospheric Studies, Evaluation Number 15, JPL Publication 06-2, Jet Propulsion Laboratory, Pasadena, available at: http://jpldataeval.jpl.nasa.gov, last access: July 2006.

Schneider, P. and van der A, R. J.: A global single-sensor analysis of 2002–2011 tropospheric nitrogen dioxide trends observed from space, J., Geophy. Res., 117, D16309, doi:10.1029/2012JD017571, 2012.

Schoeberl, M. R., Duncan, B. N., Douglass, A. R., Waters, J., Livesey, N., Read, W., and Filipiak, M.: The carbon monoxide tape recorder, Geophys. Res. Lett., 33, L12811, doi:10.1029/2006GL026178, 2006.

Schulz, M., de Leeuw, G., and Balkanski, Y.: Sea salt aerosol source functions and emissions, in: Emission of atmospheric trace compounds, Vol. 18 of the series Advances in Global Change Research, edited by: Granier, C., Artaxo, P., and Reeves, C., Springer, the Netherlands, 333–359, doi:10.1007/978-1-4020-2167-1_9, 2004.

Schultz, M. G., Heil A., Hoelzemann, J. J., Spessa, A., Thonicke, K., Goldammer, J., Held, A. C., Pereira, J. M., and Van Het Bolscher, M.: Global Wildland Fire Emissions from 1960 to 2000, Global Biogeochem. Cy., 22, GB2002, doi:10.1029/2007GB003031, 2005.

Schultz, M. G., Backman, L., Balkanski, Y., Bjoerndalsaeter, S., Brand, R., Burrows, J., Dalsoeren, S., de Vasconcelos, M., Grodtmann, B., Hauglustaine, D., Heil, A., Hoelzemann, J., Isaksen, I., Kaurola, J., Knorr, W., Ladstaetter-Weienmayer, A., Mota, B., Oom, D., Pacyna, J., Panasiuk, D., Pereira, J., Pulles, T., Pyle, J., Rast, S., Richter, A., Savage, N., Schnadt, C., Schulz, M., Spessa, A., Staehelin, J., Sundet, J., Szopa, S., Thonicke, K., van het Bolscher, M., van Noije, T., van Velthoven, P., Vik, A., and Wit-

trock, F.: REanalysis of the TROpospheric chemical composition over the past 40 years (RETRO). A long-term global modeling study of tropospheric chemistry, Final Report, Tech. rep., Max Planck Institute for Meteorology, Hamburg, Germany, 2007.

Schultz, M. G., Heil, A., Hoelzemann, J. J., Spessa, A., Thonicke, K., Goldammer, J. G., Held, A. C., Pereira, J. M. C., and van het Bolscher, M.: Global wildland fire emissions from 1960 to 2000, Global Biogeochem. Cy., 22, GB2002, doi:10.1029/2007GB003031, 2008.

Sillman, S.: The use of NO_y, H_2O_2, and HNO_3 as indicators for ozone-NO_x-hydrocarbon sensitivity in urban locations, J. Geophys. Res., 100, 14175–14188, doi:10.1029/94JD02953, 1995.

Sinha, V., Kumar, V., and Sarkar, C.: Chemical composition of pre-monsoon air in the Indo-Gangetic Plain measured using a new air quality facility and PTR-MS: high surface ozone and strong influence of biomass burning, Atmos. Chem. Phys., 14, 5921–5941, doi:10.5194/acp-14-5921-2014, 2014.

Søvde, O. A., Hoyle, C. R., Myhre, G., and Isaksen, I. S. A.: The HNO_3 forming branch of the $HO_2 + NO$ reaction: pre-industrial-to-present trends in atmospheric species and radiative forcings, Atmos. Chem. Phys., 11, 8929–8943, doi:10.5194/acp-11-8929-2011, 2011.

Stevenson, D. S., Young, P. J., Naik, V., Lamarque, J.-F., Shindell, D. T., Voulgarakis, A., Skeie, R. B., Dalsoren, S. B., Myhre, G., Berntsen, T. K., Folberth, G. A., Rumbold, S. T., Collins, W. J., MacKenzie, I. A., Doherty, R. M., Zeng, G., van Noije, T. P. C., Strunk, A., Bergmann, D., Cameron-Smith, P., Plummer, D. A., Strode, S. A., Horowitz, L., Lee, Y. H., Szopa, S., Sudo, K., Nagashima, T., Josse, B., Cionni, I., Righi, M., Eyring, V., Conley, A., Bowman, K. W., Wild, O., and Archibald, A.: Tropospheric ozone changes, radiative forcing and attribution to emissions in the Atmospheric Chemistry and Climate Model Intercomparison Project (ACCMIP), Atmos. Chem. Phys., 13, 3063–3085, doi:10.5194/acp-13-3063-2013, 2013.

Stier, P., Feichter, J., Kinne, S., Kloster, S., Vignati, E., Wilson, J., Ganzeveld, L., Tegen, I., Werner, M., Balkanski, Y., Schulz, M., Boucher, O., Minikin, A., and Petzold, A.: The aerosol-climate model ECHAM5-HAM, Atmos. Chem. Phys., 5, 1125–1156, doi:10.5194/acp-5-1125-2005, 2005.

Thuburn, J. and Craig, G. C.: On the temperature structure of the tropical substratosphere, J. Geophys. Res.-Atmos., 107, D24017, doi:10.1029/2001JD000448, 2002.

Tie, X., Madronich, S., Li, G .H., Ying, Z. M., Zhang, R., Garcia, A., Lee-Taylor, J., and Liu, Y.: Characterizations of chemical oxidants in Mexico City: a regional chemical/dynamical model (WRF-Chem) study, Atmos. Environ., 41, 1989–2008, doi:10.1016/j.atmosenv.2006.10.053, 2007.

Tie, X. X., Zhang, R., Brasseur, G., Emmons, L., and Lei, W.: Effects of lightning on reactive nitrogen and nitrogen reservoir species in the troposphere, J. Geophys. Res.-Atmos., 106, 3167–3178, doi:10.1029/2000JD900565, 2001.

Tiedtke, M.: A comprehensive mass flux scheme for cumulus parameterization in large-scale models, Mon. Weather Rev., 117, 1779–1800, 1989.

Tobo, Y., Iwasaka, Y., Zhang, D., Shi, G., Kim, Y. S., Tamura, K., and Ohashi, T.: Summertime "ozone valley" over the Tibetan Plateau derived from ozonesondes and EP/TOMS data, Geophys. Res. Lett., 35, L16801, doi:10.1029/2008GL034341, 2008.

Vernier, J.-P., Fairlie, T. D., Natarajan, M., Wienhold, F. G., Bian, J., Martinsson, B. G., Crumeyrolle, S., Thomason, L. W., and Bedka, K.: Increase in upper tropospheric and lower stratospheric aerosol levels and its potential connection with Asian Pollution, J. Geophys. Res.-Atmos., 120, 1608–1619, doi:10.1002/2014JD022372, 2015.

Vinoj, V., Rasch, P. J., Wang, H., Yoon, J. H., Ma, P. L., Landu, K., and Singh, B.: Short-term modulation of Indian summer monsoon rainfall by West Asian dust, Nat. Geosci., 7, 308–313, doi:10.1038/ngeo2107, 2014.

Vogel, B., Günther, G., Müller, R., Grooß, J.-U., and Riese, M.: Impact of different Asian source regions on the composition of the Asian monsoon anticyclone and of the extratropical lowermost stratosphere, Atmos. Chem. Phys., 15, 13699–13716, doi:10.5194/acp-15-13699-2015, 2015.

Vogel, B., Günther, G., Müller, R., Grooß, J.-U., Afchine, A., Bozem, H., Hoor, P., Krämer, M., Müller, S., Riese, M., Rolf, C., Spelten, N., Stiller, G. P., Ungermann, J., and Zahn, A.: Long-range transport pathways of tropospheric source gases originating in Asia into the northern lower stratosphere during the Asian monsoon season 2012, Atmos. Chem. Phys., 16, 15301–15325, doi:10.5194/acp-16-15301-2016, 2016.

Waters, J. W., Froidevaux, L., Harwood, R. S., Jarnot, R. F., Pickett, H. M., Read, W. G., Siegel, P. H., Cofield, R. E., Filipiak, M. J., Flower, D. A., Holden, J. R., Lau, G. K., Livesey, N. J., Manney, G. L., Pumphrey, H. C., Santee, M. L., Wu, D. L., Cuddy, D. T., Lay, R. R., Loo, M. S., Perun, V. S., Schwartz, M. J., Stek, P. C., Thurstans, R. P., Boyles, M. A., Chandra, S., Chavez, M. C., Chen, G. S., Chudasama, B. V., Dodge, R., Fuller, R. A., Girard, M. A., Jiang, J. H., Jiang, Y., Knosp, B. W., LaBelle, R. C., Lee, K. A., Miller, D., Oswald, J. E., Patel, N. C., Pukala, D. M., Quintero, O., Scaff, D. M., Snyder, W. V., Tope, M. C., Wagner, P. A., and Walch, M. J.: The Earth Observing System Microwave LimbSounder (EOS MLS) on the Aura satellite, IEEE T. Geosci. Remote, 44, 1075–1092, doi:10.1109/TGRS.2006.873771, 2006.

Wild, O. and Akimoto, H.: Intercontinental transport of ozone and its precursors in a three-dimensional global CTM, J. Geophys. Res., 106, 27729–27744, doi:10.1029/2000JD000123, 2001.

Wu, G. X. and Zhang, Y. S.: Tibetan Plateau forcing and the timing of the monsoon onset over South Asia and the South China Sea, Mon. Weather Rev., 126, 913–927, doi:10.1175/1520-0493(1998)126<0913:TPFATT>2.0.CO;2, 1998.

Xiong, X., Houweling, S., Wei, J., Maddy, E., Sun, F., and Barnet, C.: Methane plume over south Asia during the monsoon season: satellite observation and model simulation, Atmos. Chem. Phys., 9, 783–794, doi:10.5194/acp-9-783-2009, 2009.

Yamaji, K., Ohara, T., Uno, I., Tanimoto, H., Kurokawa, J., and Akimoto, H.: Analysis of the seasonal variation of ozone in the boundary layer in East Asia using the Community Multiscale Air Quality model: what controls surface ozone levels over Japan?, Atmos. Environ., 40, 1856–1868, 2006.

Yanai, M., Li, C., and Song, Z.: Seasonal heating of the Tibetan Plateau and its effects on the evolution of the Asian summer monsoon, J. Meteorol. Soc. Jpn., 70, 189–221, 1992.

Zhang, R. W., Lei, X., and Hess, T. P.: Industrial emissions cause extreme diurnal urban ozone variability, P. Natl. Acad. Sci. USA, 101, 6346–6350, doi:10.1073/pnas.0401484101, 2004.

Zhao, B., Wang, S. X., Liu, H., Xu, J. Y., Fu, K., Klimont, Z., Hao, J. M., He, K. B., Cofala, J., and Amann, M.: NO_x emissions in

China: historical trends and future perspectives, Atmos. Chem. Phys., 13, 9869–9897, doi:10.5194/acp-13-9869-2013, 2013.